Prediction of boron transient enhanced diffusion through the atom-by-atom modeling of extended defects

E. Lampin, Fuccio Cristiano, Y. Lamrani, Alain Claverie, B. Colombeau, N.E.B. Cowern

Prediction of boron transient enhanced diffusion through the atom-by-atom modeling of extended defects

Cite as: Journal of Applied Physics **94**, 7520 (2003); https://doi.org/10.1063/1.1627461
Submitted: 01 August 2003 • Accepted: 23 September 2003 • Published Online: 02 December 2003

E. Lampin, F. Cristiano, Y. Lamrani, et al.

Prediction of boron transient enhanced diffusion through the atom-by-atom modeling of extended defects

E. Lampin[a)]
IEMN/ISEN, UMR CNRS 8520, 59652 Villeneuve d'Ascq, Cedex, France

F. Cristiano, Y. Lamrani, and A. Claverie
Ion Implantation Group, CEMES/LAAS-CNRS, 31055 Toulouse, France

B. Colombeau and N. E. B. Cowern
Advanced Technology Institute, University of Surrey, Guildford, GU2 7XH Surrey, United Kingdom

(Received 1 August 2003; accepted 23 September 2003)

The modeling of the atom-by-atom growth of extended defects is coupled to the diffusion equations of boron by transferring the free interstitial supersaturation calculated with a defect model into a process simulator. Two methods to achieve this coupling (equilibrium method and fully coupled method, respectively) are presented and tested against a variety of experimental conditions. They are first applied to a transient enhanced diffusion experiment carried out on a structure containing several B delta-doped layers, in which the amount of diffusion of the different layers is accurately predicted. The fully coupled method is then used to simulate the diffusion of ultrashallow B-implanted profiles. This work definitely demonstrates the relevance of accurate physical defect models for the successful design of ultrashallow junctions in future generations of integrated circuits. © *2003 American Institute of Physics.* [DOI: 10.1063/1.1627461]

I. INTRODUCTION

The transient enhanced diffusion (TED) of ion-implanted boron in silicon is a major problem in the fabrication of ultrashallow junctions (USJs) for advanced integrated circuits (ICs). It is now well established that boron diffuses predominantly by a kick-out mechanism in silicon,[1] that is, via Si self-interstitials, Si_{int}s. The boron diffusion enhancement with respect to thermal equilibrium, D_B/D_B^*, is thus equal to the supersaturation S of Si_{int}s in the implanted region during annealing:

$$\frac{D_B}{D_B^*}=\frac{C_I}{C_I^*}=S. \tag{1}$$

When extended defects form upon annealing, the value of S is governed by the dynamical equilibrium between the free Si_{int}s and the different types of extended defects. Indeed, the extended defects capture and release Si_{int}s during their evolution, therefore maintaining a high Si_{int}s supersaturation in the surrounding region. Depending on the experimental conditions, these extended defects can grow from small interstitial clusters to {113} defects and up to dislocation loops. Many research works have been dedicated to the understanding and modeling of the defect formation and evolution in the recent years, and several predictive computer models have been proposed in the literature.[2–8] However, no results have been reported so far on the direct influence of extended defects on boron diffusion; the tests against experimental studies have concerned either the calculation of boron diffusion length at a given concentration level or the calculation of the extracted Si_{int}s supersaturation from secondary ion mass spectrometry (SIMS) measurements of B diffused profiles. Indeed, none of these models has yet been implemented in a process simulator to predict the whole B concentration profile after diffusion.

In this article, we propose two different approaches for the transfer of a defect model into a process simulator. The CEMES[9] defect model[7] is first used to describe the extended defect evolution. In this model, the formation energy and the capture efficiency associated with each type of defect are theoretically calculated on the basis of their crystallographic configuration. This allows the formation and evolution of the defects to be predicted using a single fitting parameter. The Si_{int}s supersaturation level calculated in this way is then inserted as an input into a B diffusion solver. Two methods to achieve this coupling (equilibrium method and fully coupled method, respectively) will be presented and tested against a variety of experimental conditions. While representing a further validation of the CEMES model, this work will definitely demonstrate the relevance of accurate physical defect models for the successful design of USJs in future generations of ICs.

The essential of the CEMES model is reviewed in Sec. II. The two approaches for the coupling to the equations of B diffusion are presented in Sec. III. Two applications of these approaches will then be presented: the first to the study of the diffusion of ''delta-doped'' boron marker layers (Sec. IV) and the second to that of ultrashallow boron-implanted profiles (Sec. V).

II. MODELING OF THE EXTENDED DEFECTS

The approach used to describe the kinetics of the extended defects is the CEMES method presented in Ref. 7. The model is based on a set of $(n+1)$ coupled differential

a)Electronic mail: evelyne.lampin@isen.iemn.univ-lille1.fr

equations. The first n equations describe the flux of atoms from defects containing n atoms to defects containing $n+1$ and $n-1$ atoms:

$$\frac{dN_n}{dt} = F_{n-1}N_{n-1} - F_nN_n + R_{n+1}N_{n+1} - R_nN_n, \tag{2}$$

where N_n is the number of precipitates of size n.

The emission rate (R_n) and the capture rate (F_n) are calculated assuming a diffusion-limited growth of the defects. R_n and F_n both depend on the defect geometry through a term that includes the defect capture efficiency (A_n/R_{eff}), A_n being the capture area of the defect and R_{eff} the radial extension of the diffusion field around it. In addition, R_n also depends on the defect stability through its formation energy $E_f(n)$, and is thus given by

$$R_n = D_I C_I^* \left(\frac{A_n}{R_{\text{eff}}}\right) \exp\left[\frac{E_f(n)}{kT}\right], \tag{3}$$

where $D_I C_I^*$ is the self-diffusivity of the Si_{int}s, while the capture rate F_n is proportional to the supersaturation of Si_{int}s in the defect region (S_{def}), and is thus given by

$$F_n = D_I C_I^* \left(\frac{A_n}{R_{\text{eff}}}\right) S_{\text{def}}. \tag{4}$$

While growing, it is found experimentally that the defects evolve from clusters to {113}s, and to perfect and faulted dislocation loops.[7] As a consequence, the formation energy [$E_f(n)$] and the capture efficiency [A_n/R_{eff}] have different formulations depending on the defect size. For $n<10$ (clusters), the oscillating formation energies obtained by Cowern *et al.*[5] with stable configurations for four and eight atoms are used. When n increases, such formation energies tend towards values expected for small {113} defects. The formation energy of the {113}s is taken from Colombeau *et al.*[10] and tends towards 0.65 eV for large sizes. The formation energies of the dislocation loops are given in Ref. 11. Detailed information concerning the different values of the capture efficiency as a function of the defect size are given in Refs. 7 and 12.

The evolution of the Si_{int}s supersaturation in the defect region (S_{def}) not only depends on the capture and release of Si_{int}s by the extended defects, but also on their diffusion towards the bulk and towards the surface. The equation for the free Si_{int}s gives in steady state

$$0 = \frac{dC_I}{dt} = -J_{\text{surf}} + J_{\text{bulk}} + \sum_{n=2}^{\infty} (\beta_n R_n - F_n) N_n. \tag{5}$$

The first term (J_{surf}) is the flux of interstitials towards the surface. The surface is assumed to be a perfect sink for interstitials. Its trapping efficiency is described in terms of the surface recombination length (L_{surf}), that is the mean free path traveled on the surface by a Si interstitial atom before recombining. The surface recombination length is an intrinsic characteristic of the wafer surface and depends only on the annealing ambient (number of available traps) and temperature (Si_{int}s diffusivity). This boundary condition induces a gradient of the free interstitial concentration between the defect region and the surface, and by consequence a flux of interstitials J_{surf} towards the surface. This is schematically represented in Fig. 1, where L_{surf} appears as a fictitious distance above the surface at which the supersaturation goes back to the equilibrium level. A linear increase of the Si_{int}s concentration profile from $-L_{\text{surf}}$ to the depth at which the defects are located (z_{def}) is assumed in the model. The validity of this assumption is demonstrated in Sec. IV. The flux (J_{surf}) is under this assumption:

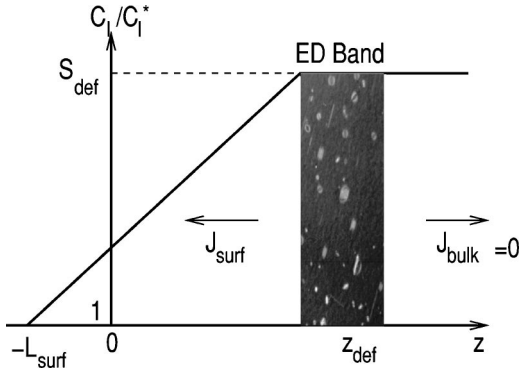

FIG. 1. Schematic representation of the band of extended defects (ED band) and of the flux of Si_{int}s towards the surface and the depth of the wafer.

$$J_{\text{surf}} = D_I \frac{C_I^*(S_{\text{def}} - 1)}{L_{\text{surf}} + z_{\text{def}}}. \tag{6}$$

The very low concentration of Si_{int}s traps in the bulk of the structures used in this study [chemical-vapor-deposition (CVD)-grown layers or Czochralski Si wafers] results in a quasiconstant Si_{int}s supersaturation level below the defect region. The flux towards the depth of the wafer (J_{bulk}) in Eq. (5) is thus neglected.

The third term in Eq. (5) gives the capture and emission of Si atoms by the extended defects. The factor β_n is the number of Si atoms released by the break-up of an atom from a defect of size n, that is, $\beta=2$ for $n=2$, $\beta=1$ otherwise. From Eqs. (5) and (6), the following equation is obtained for S_{def}:

$$S_{\text{def}} = \frac{\Sigma_{n=2}^{\infty} \beta_n R_n N_n + D_I C_I^*/(L_{\text{surf}} + z_{\text{def}})}{D_I C_I^* \left(\dfrac{1}{L_{\text{surf}} + z_{\text{def}}} + \Sigma_{n=2}^{\infty} \dfrac{A_n}{R_{\text{eff}}} N_n\right)}. \tag{7}$$

In order to reduce the computational effort, the $n+1$ equations [Eqs. (2) and (7)] are only solved at $z=z_{\text{def}}$, the depth where the extended defects are located.

With the exception of the surface recombination length L_{surf}, the different types of extended defects are described in the model without any free parameters. Its predictive capabilities have already been demonstrated for the evolution of both {113} defects and free Si_{int}s supersaturation measurements.[7,10]

III. COUPLING WITH THE BORON DIFFUSION EQUATIONS

In order to reproduce the evolution of the entire B concentration profiles during annealing, the Si_{int}s supersaturation calculated with the CEMES model [$S_{\text{def}}(t)$] is coupled with

the equations of B diffusion within the process simulator IMPACT.[13–15] The major problem is to expand the zero-dimensional result (S_{def} is calculated at the single point z_{def}) into a one-dimensional Si_{int}s profile. We followed two different methods.

In the first method (hereafter called equilibrium method), we take the assumptions used to draw Fig. 1 to determine an analytical expression of $S(z)$:

$$S(z)=[z(S_{\text{def}}-1)+z_{\text{def}}+S_{\text{def}}L_{\text{surf}}]/(z_{\text{def}}+L_{\text{surf}}) \quad \text{for} \quad z<z_{\text{def}},$$
$$=S_{\text{def}} \quad \text{for} \quad z>z_{\text{def}}. \tag{8}$$

We use this function $S(z)$ to scale the B diffusivity in an equilibrium diffusion scheme:

$$\frac{\partial C_{\text{B}}}{\partial t}=\nabla(D_{\text{B}}\nabla C_{\text{B}}), \tag{9}$$

with

$$D_{\text{B}}=D_{\text{B}}^{*}S(z), \tag{10}$$

and taking as a reference an equilibrium boron diffusivity value of 0.757 $\text{cm}^2/\text{s}\ \exp(-3.46\ \text{eV}/kT)$.[16]

In the second method (hereafter called fully coupled method), the full interactions between dopants and point defects are solved. Instead of imposing a predetermined ''shape'' for the depth distribution of the Si_{int}s supersaturation, as in the equilibrium method, a source/sink term (GR_{def}) is added to the diffusion equation of free interstitials in order to make the supersaturation level (at $z=z_{\text{def}}$) equal to S_{def} (as calculated with the CEMES model) at any time during annealing. Apart from this boundary condition, the Si_{int}s are free to diffuse and interact with the B atoms eventually present in the surrounding region. The final depth distribution of Si_{int}s will therefore depend on this source/sink term, on their diffusion, on their recombination at the surface, and on their coupling with B. The source/sink term (GR_{def}) that accounts for the emission or capture of interstitials from the defect band is written as follows:

$$GR_{\text{def}}(z=z_{\text{def}})=h_{\text{def}}(C_{\text{I}}-S_{\text{def}}C_{\text{I}}^{*}) \quad \text{at} \quad z=z_{\text{def}}, \tag{11}$$

where h_{def} is the velocity at which C_{I} tends towards $S_{\text{def}}C_{\text{I}}^{*}$ and is set to a high value. The diffusion equation for the interstitials is therefore

$$\frac{\partial C_{\text{I}}}{\partial t}=\nabla(D_{\text{I}}\nabla C_{\text{I}})-GR_{\text{KO}}+GR_{\text{def}}(z=z_{\text{def}}), \tag{12}$$

where GR_{KO} is the generation/recombination term of the kick-out coupling of interstitials with B atoms.[13] The surface boundary condition for this equation is written in terms of the surface recombination length:

$$-L_{\text{surf}}\nabla C_{\text{I}}+(C_{\text{I}}-C_{\text{I}}^{*})=0. \tag{13}$$

Finally, the diffusion equation for the interstitial mobile boron atoms (B_{int}) is written as

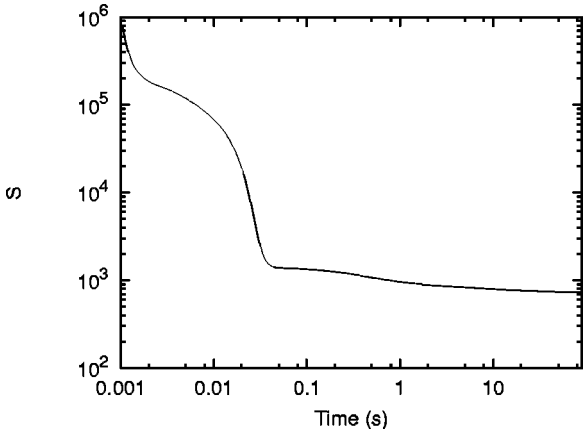

FIG. 2. Si interstitial supersaturation at $z_{\text{def}}=300$ nm during annealing at 850 °C calculated with the CEMES model. Implant conditions: 100 keV Si^+ ions to a dose of $2\times10^{14}\ \text{cm}^{-2}$.

$$\frac{\partial C_{\text{B}_{\text{int}}}}{\partial t}=\nabla(D_{\text{B}_{\text{int}}}\nabla C_{\text{B}_{\text{int}}})+GR_{\text{KO}}, \tag{14}$$

where $D_{\text{B}_{\text{int}}}$ is the B_{int} diffusion coefficient.

IV. APPLICATION 1: TED IN A STRUCTURE CONTAINING B DELTA-LAYERS

In this section, the model presented in Secs. II and III has been used to simulate the results of a TED experiment run on Si structures containing four B marker layers implanted with 100 keV Si^+ ions to a dose of $2\times10^{14}\ \text{cm}^{-2}$ (nonamorphizing implant) and annealed at 850 °C for 15, 30, 60, or 90 s. Si implantation is performed in order to generate an initial Si_{int}s supersaturation, while the B peaks are used to probe the amount of TED at different depths of the substrate.

Transmission electron microscopy analysis after annealing (not shown) indicates that a layer of {113} defects is formed between 0.15 and 0.45 μm.[17] The second boron marker layer is therefore entirely located within the defect region. For the calculation of the supersaturation S_{def} at 850 °C with the CEMES model, the defect depth z_{def} has been set at 300 nm. Results are shown in Fig. 2. In the early stages of the annealing process ($t<0.1$ s), the supersaturation exhibits a fast decrease from a level of about 10^6 down to a ''quasiplateau'' at about 10^5, due to the presence of very small clusters.[18] The second plateau at values around 1000 is instead typical of the dynamical equilibrium of Si_{int}s with {113} defects.

Subsequently, the B and Si_{int}s depth profiles are calculated with IMPACT for annealing at 850 °C for 15, 30, 60, and 90 s. The surface recombination length (L_{surf}) has been neglected in these calculations ($L_{\text{surf}}=0$) due to the fact that no boron is present at the silicon surface while the defects are deep in the structure (300 nm). Under these conditions, the surface recombination length, which is typically of the order of few nanometers, has no impact on the simulation results.

A. Equilibrium method

Figure 3 shows the resulting simulated B profiles (solid lines) compared with the experimental data (symbols) when

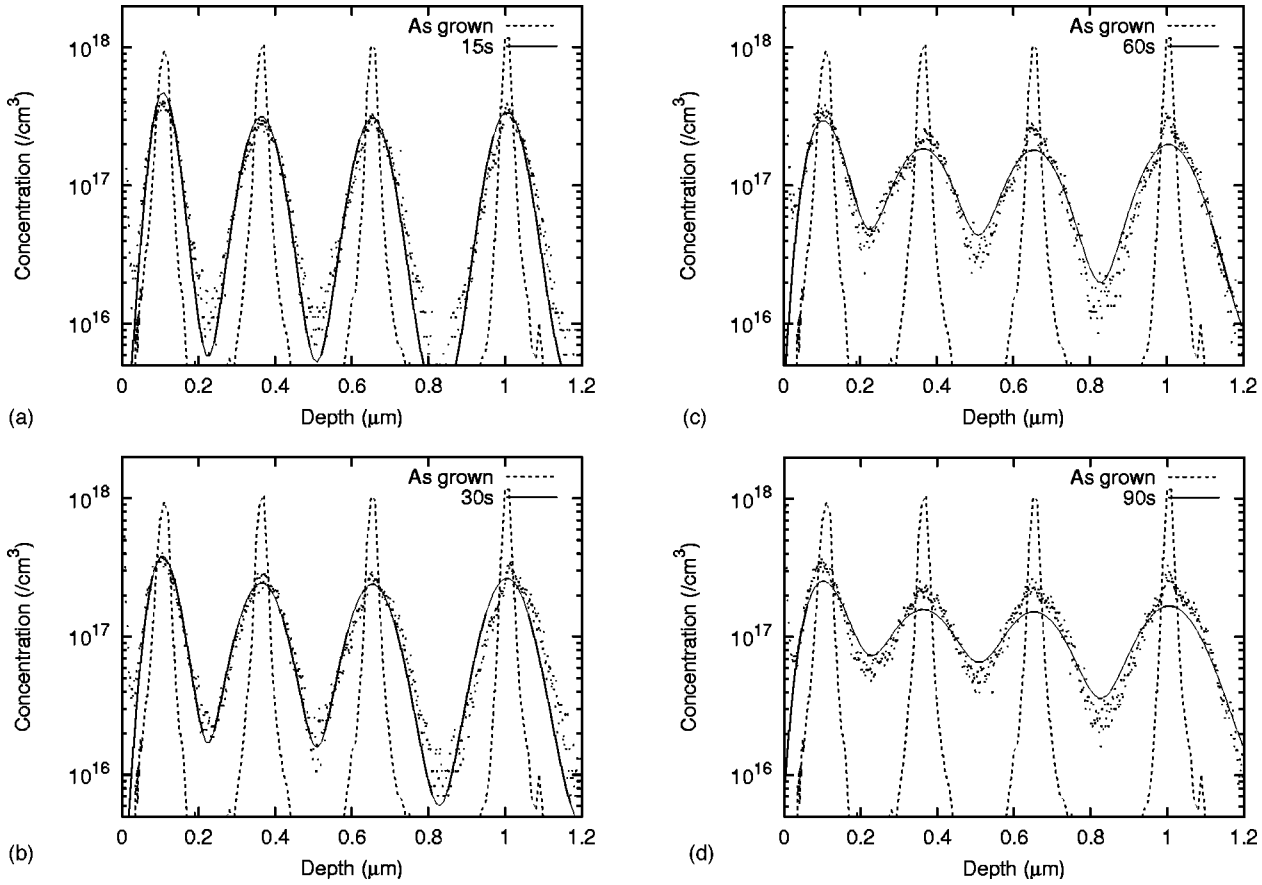

FIG. 3. Boron concentration profiles after annealing at 850 °C for 15 s (a), 30 s (b), 60 s (c) and 90 s (d). Dashed lines: reference as-grown profiles. Dotted lines: measured profiles (SIMS). Solid lines: simulated profiles (equilibrium method).

using the equilibrium method. It has to be noted that once a value of L_{Surf} has been fixed, there are no free parameters in the simulation of the B profile. The excellent agreement with the experiments thus validates the amplitude of the supersaturation calculated with the CEMES model. In addition, the analytical formulation of the supersaturation $S(z)$ [Eq. (8)] clearly succeeds in giving the evolution of B diffusion with depth; Fig. 3 shows that the smaller enlargement of the peak closer to the surface is simulated throughout the annealing. More generally, this agreement directly validates the physical mechanism proposed to explain TED:[19,20] the Ostwald ripening of extended defects in conjunction with the surface proximity effect are responsible for the supersaturation at the origin of the enhancement of B diffusion.

B. Fully coupled method

The analytical expression of $S(z)$—in particular, the linear increase from the surface to z_{def}—has also been validated by using the fully coupled method. Figure 4 shows the corresponding depth profile of B and $\mathrm{Si_{int}}$s after 30 s. The agreement of the B profiles with the experiment has the same quality as that with the equilibrium model. In particular, the flat $\mathrm{Si_{int}}$s profile below the defect region (see Fig. 4) is the result of the assumption that no $\mathrm{Si_{int}}$s traps are present in the bulk of high-quality CVD layers. The good agreement with the measured B profiles clearly justifies this choice. On the other hand, the gradient in the $\mathrm{Si_{int}}$s concentration profile between the defect region and the surface exhibits a linear decrease (as shown in Fig. 5, plotted using a linear concentration scale), therefore validating the assumption used to write the depth distribution of the $\mathrm{Si_{int}}$s supersaturation in the equilibrium method [Eq. (8)]. The validation of the approach and of the numerical modeling of the extended defects is demonstrated with the two methods. In the next section, we

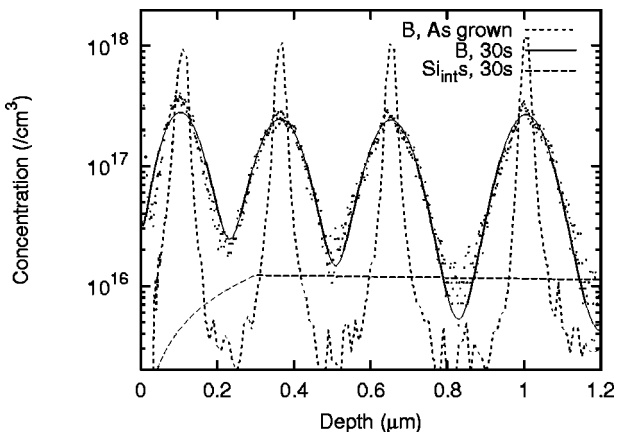

FIG. 4. B and $\mathrm{Si_{int}}$s profiles after annealing at 850 °C for 30 s. Dashed line: reference as-grown profile. Dotted lines: measured profile (SIMS). Solid line: simulated profiles (fully coupled method). The points are the measurements. The lines are the simulations with the full coupled model. Long-dashed line: $\mathrm{Si_{int}}$s profile.

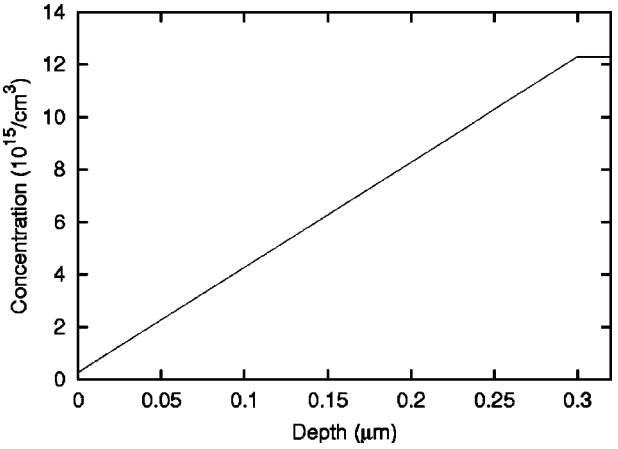

FIG. 5. Simulated Si_{int}s profile (linear time-scale) after annealing at 850 °C for 30 s.

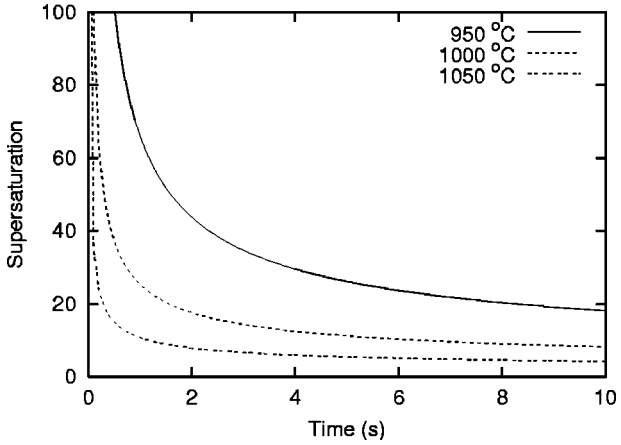

FIG. 6. Si interstitial supersaturation at $z_{def}=175$ nm during annealing at 950, 1000, and 1050 °C calculated with the CEMES model. Implant conditions: 150 keV Ge^+ ions to a dose of 2×10^{15} cm^{-2}.

will apply the fully coupled method (that more accurately describes the out-of-equilibrium point defect–dopant interactions) to model the diffusion of ultralow-energy B-implanted profiles.

V. APPLICATION 2: TED AFTER ULTRALOW-ENERGY B^+ IMPLANTS

We now consider the case of an ultrashallow $p-n$ junction obtained by implanting B^+ ions into a preamorphized wafer. B is implanted at 1 keV to a dose of 3×10^{14} cm^{-2} into a wafer initially preamorphized by a 150 keV Ge^+ implant to a dose of 2×10^{15} cm^{-2}, leading to the formation of a surface amorphous layer of about 175 nm. After implantation, the samples were annealed for 10 s at 950, 1000, or 1050 °C in a nitrogen ambient. At these annealing temperatures, the end-of-range defect layer formed below the amorphous/crystalline (a/c) interface consists of dislocaton loops.[21] Similarly to the previous case, the CEMES model is first used to calculate the time evolution of the Si_{int}s supersaturation at 950, 1000, and 1050 °C. For the calculations, the extended defects are assumed to be located at the depth of the a/c interface ($z_{def}=175$ nm). The surface recombination length (L_{surf}) has been set at 0.8, 1.8, and 3.9 nm, for annealing temperatures of 950, 1000, and 1050 °C, respectively; that is, L_{surf} is thermally activated with the same activation energy as the Si_{int}s diffusivity, in agreement with previous studies.[18] The calculated supersaturations are shown in Fig. 6 for the different temperatures. In contrast with the previous application, the Si_{int}s supersaturation rapidly decreases to values around 10 already after 10 s of annealing, which is typical of the Ostwald ripening of dislocation loops. Indeed, dislocation loops are more energetically stable than {113} defects and induce a much lower Si_{int}s supersaturation in their surroundings.[21] The calculated supersaturations, presented in Fig. 6, are then coupled to the boron diffusion equations via the fully coupled method. Figure 7 shows the resulting boron simulated profiles (lines) together with the measured ones (symbols) for the different annealing temperatures. An excellent agreement is obtained for all cases. Clearly, the characteristic features used in the physical model to describe the evolution of clusters, {113}s and dislocation loops (including their formation energies and capture efficiencies) allow to accurately predict the diffusion of ultralow-energy boron-implanted profiles.

The results presented in the last two sections confirm that a single physical mechanism (Ostwald ripening) is responsible for the evolution of the Si_{int}s supersaturation (and hence of TED) in presence of any type of extended defects in ion implanted silicon (i.e., interstitial clusters, {113}s and dislocation loops). In addition, they show that a ''unified'' model can be used to describe the concomitant evolution of the defects and of the Si_{int}s supersaturation after both nonamorphizing and amorphizing implants.

VI. CONCLUSION

In this article, the modeling of the atom-by-atom growth of extended defects is coupled to the diffusion equations of boron by transferring the free interstitial supersaturation calculated with a defect model into a process simulator. The approach is first applied to a TED experiment carried out on a structure containing several B delta-doped layers, in which the amount of diffusion of the different layers is accurately

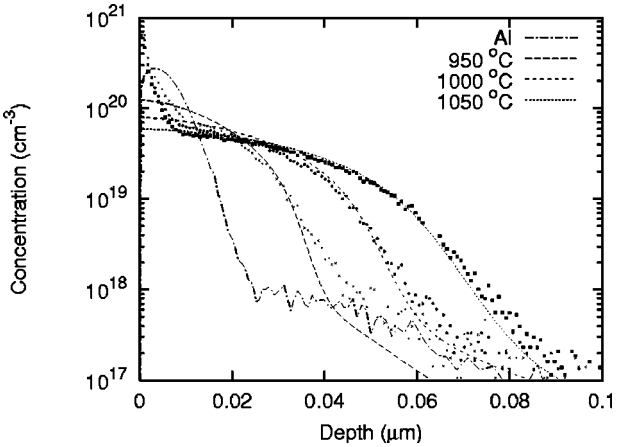

FIG. 7. Boron concentration profiles after implantation and annealing for 10 s at 950, 1000, and 1050 °C, respectively. Symbols: measured profiles (SIMS). Lines: simulated profiles (fully coupled method).

predicted. The approach is then successfully used to simulate the diffusion of ultrashallow B-implanted profiles. This work confirms that a ''unified'' model can be used to describe the concomitant evolution of all defect types and of the Si_{int}s supersaturation after both nonamorphizing and amorphizing implants. As a consequence, it definitely demonstrates the relevance of accurate physical defect models for the design of ultrashallow junctions in future generations of ICs.

VII. ACKNOWLEDGMENTS

This work is part of the FRENDTECH project and is funded by the European Community as IST/2000-30129. We thank the CICT (Center Interuniversitaire de Calcul de Toulouse) for providing access to their computing facilities and Dr. H. Schaefer from Infineon Technologies for providing the B marker layers.

[1] P. M. Fahey, P. B. Griffin, and J. D. Plummer, Appl. Phys. Lett. **61**, 289 (1989).
[2] H. S. Chao, P. B. Griffin, J. D. Plummer, and C. S. Rafferty, Appl. Phys. Lett. **69**, 2113 (1996).
[3] A. H. Gencer and S. T. Dunham, J. Appl. Phys. **81**, 631 (1997).
[4] G. Hobler and C. S. Rafferty, Mater. Res. Soc. Symp. Proc. **568**, 123 (1999).
[5] N. E. B. Cowern, G. Mannino, P. A. Stolk, F. Roozeboom, H. G. A. Huizing, J. G. M. van Berkum, W. B. de Boer, F. Cristiano, A. Claverie, and M. Jaraiz, Phys. Rev. Lett. **82**, 4460 (1999).
[6] M. Law and K. S. Jones, Tech. Dig. - Int. Electron Devices Meet. **2000**, 551.
[7] A. Claverie, B. Colombeau, B. de Mauduit, C. Bonafos, X. Hebras, G. Ben Assayag, and F. Cristiano, Appl. Phys. A: Mater. Sci. Process. **76**, 1025 (2003).
[8] M. Aboy, L. Pelaz, L. A. Marques, L. Enriquez, and J. Barbolla, J. Appl. Phys. **94**, 1013 (2003).
[9] The CEMES (Centre d'Elaboration de Matériaux et d'Etudes Structurales) in Toulouse, France, is the laboratory of the authors of the model (see Ref. 7).
[10] B. Colombeau, F. Cristiano, A. Altibelli, C. Bonafos, G. Ben Assayag, and A. Claverie, Appl. Phys. Lett. **78**, 940 (2001).
[11] F. Cristiano, J. Grisolia, B. Colombeau, M. Omri, B. de Mauduit, A. Claverie, L. F. Giles, and N. E. B. Cowern, J. Appl. Phys. **87**, 8420 (2000).
[12] B. Colombeau, PhD thesis, Toulouse, France, 2001.
[13] Process simulation tool developed at IEMN (Institut d'Electronique, de Microélectronique et de Nanoélectronique) in Lille, France.
[14] B. Baccus and E. Vandenbossche, Defect Diffus. Forum **115–116**, 55 (1994).
[15] E. Lampin, V. Senez, and A. Claverie, J. Appl. Phys. **85**, 8137 (1999).
[16] R. B. Fair, in *Impurity Doping Processes in Si*, edited by F. F. Y. Wang (North-Holland, Amsterdam, 1981), p. 315.
[17] B. Colombeau, N. E. B. Cowern, F. Gristiano, P. Calvo, N. Cherkashin, Y. Lamrani, and A. Claverie, Appl. Phys. Lett. **83**, 1953 (2003).
[18] N. E. B. Cowern, D. Alquier, M. Omri, and A. Claverie, Nucl. Instrum. Methods Phys. Res. B **148**, 257 (1999).
[19] C. Bonafos, M. Omri, B. de Mauduit, G. Ben Assayag, A. Claverie, D. Alquier, A. Martinez, and D. Mathiot, J. Appl. Phys. **82**, 2855 (1997).
[20] A. Claverie, L. F. Giles, M. Omri, B. de Mauduit, G. Ben Assayag, and D. Mathiot, Nucl. Instrum. Methods Phys. Res. B **147**, 1 (1999).
[21] A. Claverie, B. Colombeau, G. Ben Assayag, C. Bonafos, F. Cristiano, M. Omri, and B. de Mauduit, Mater. Sci. Semicond. Process. **3**, 269 (2000).